A third 1415 MHz survey with the Westerbork Synthesis Radio Telescope - The 5C2 region. I

Katgert, P.

Astron. & Astrophys. 38, 87 – 104 (1975)

A Third 1415 MHz Survey with the Westerbork Synthesis Radio Telescope: the 5C2 Region (Part I)

P. Katgert
Sterrewacht Leiden*

Received August 20, 1974

Summary. The 5C2 region, observed originally with the Cambridge One-Mile Telescope at 408 MHz, has been reobserved at 1415 MHz. The resulting source list contains 238 sources with attenuated flux densities exceeding the catalogue limit of 6.25 m.f.u. Out of a total of 190 5C2 sources (i.e. all 5C2 sources within the 10 dB attenuation contour of the present survey) 128 were detected with flux densities above the catalogue limit. Another 22 5C2 sources were detected with flux densities below the catalogue limit.
A discussion is given of the procedures used for determining source parameters. Special attention has been given to the determination of flux density and angular size, as well as to the question of completeness of the source list as a function of flux density *and* angular size. Below attenuated flux densities of about 12.5 m.f.u. both systematic underestimation of flux densities and selection against extended sources cannot be neglected and must be accounted for.
A detailed discussion of source counts, spectral index distributions and angular size distributions will be given in a following paper.

Key words: radio source survey — flux densities and angular sizes of extended sources — completeness of source list

I. Introduction

This is the first of two papers dealing with a 1415 MHz survey of the 5C2 region ($\alpha = 11^h00^m$, $\delta = 49°40'$), carried out with the Westerbork Synthesis Radio Telescope.
The two main reasons for carrying out this survey were a) to produce an accurately defined radio source catalogue with a limiting flux density of the order of 1 m.f.u. ($= 10^{-29}$ W m^{-2} Hz^{-1}) at a frequency of 1415 MHz and b) to obtain spectral index information for a well-defined sample of weak radio sources (hence the selection of the 5C2 region which was earlier observed at a frequency of 408 MHz, cf. Pooley and Kenderdine, 1968).
In order to reach a flux density limit of about 1 m.f.u. and, at the same time, detect as many 5C2 sources as possible the survey was divided into two parts. In the central part of the 5C2 region two fields were observed for sixteen twelve hour periods each. The results of these observations (with a limiting flux density of about 1.4 m.f.u.) will be discussed in a second paper (Le Poole, in preparation).
In this paper we present and discuss the results of twenty-four fields (observed for twelve hours each) which cover all of the 5C2 region except the central part. The total solid angle covered by these twenty-four fields is $5.52\,10^{-3}$ steradians of which $3.24\,10^{-3}$ steradians lie within the 7 dB attenuation contour of the 408 MHz 5C2 observations. The limiting attenuated flux density (i.e. the completeness limit) of the source catalogue is 6.25 m.f.u. for non-extended sources, and degrades to 12.5 m.f.u. for sources with an equivalent diameter larger than about 26″.
The present survey will provide radio source count data up to source densities that exceed the maximum source density of the 5C2 survey (Pooley and Ryle, 1968). These 1415 MHz radio source counts will be discussed in a third paper (Katgert, in preparation), together with other radio statistics derived from this survey (such as angular diameter distribution, spectral index distribution etc.).
It will be clear that, due to the quality of the radio positions (which is generally better than 2–3″), the present survey is a valuable basis for systematic deep optical identifications of weak radio sources. In our opinion such radio surveys merit a considerable effort on the part of optical astronomers to try and obtain deep optical identifications either by direct photography or by more advanced optical detection techniques. Recent work by Katgert (J.K.) and Spinrad (1974) shows that such efforts may indeed yield a large gain in identification percentage.

II. Observations and Calibration

The observations were done between the end of January and the beginning of April 1971. The sensitivity centres of the twenty-six fields were chosen such as to enable

* Now at Institute of Astronomy, Cambridge, U.K.

Table 1. Sensitivity centres of the twenty-four fields

No.	α(1950)	δ(1950)	No.	α(1950)	δ(1950)
1	$10^h50^m06^s$	50°57′30″	13	$11^h00^m09^s$	50°50′30″
2	10 50 30	49 59 30	14	11 00 57	52 40 30
3	10 51 06	47 58 00	15	11 02 09	47 24 00
4	10 51 57	49 06 00	16	11 04 45	48 08 30
5	10 55 18	48 43 00	17	11 04 45	49 45 30
6	10 55 24	50 26 00	18	11 05 03	50 43 00
7	10 56 03	49 40 30	19	11 06 03	51 29 30
8	10 56 03	52 12 00	20	11 07 45	48 49 00
9	10 56 18	51 19 00	21	11 09 15	50 26 30
10	10 57 54	47 49 30	22	11 09 36	49 36 30
11	10 59 15	48 33 00	23	11 09 42	51 21 00
12	10 59 27	49 18 30	24	11 11 48	48 29 00

detection of essentially all 5C2 sources whose spectral indices (between 408 and 1415 MHz) are larger than about -0.7. Moreover, we tried to avoid the presence of strong sources near the field centres in order to minimize the dynamic range requirements. The sensitivity centres of the twenty-four single twelve hour period fields are given in Table 1.

All observations have been done with the movable telescopes at distances of 54 and 126 m from the nearest fixed one. The measured baselines therefore range from 54 to 1422 m (255 to 6707 λ). The increment between consecutive baselines is 72 m (340 λ), which results in elliptical grating responses with semi minor axes of 10′, 20′ etc.

During the survey the instrument was operated in its twelve hour period observing mode, i.e. all observations extend over a full 180 degrees of hour angle. When part of an observation had to be discarded due to external or internal interference it was reobserved.

In these observations the dipoles in the two movable telescopes were parallel to those in the ten fixed telescopes, i.e. all dipoles were in position angles of either 0 or 90 degrees. The four polarization channels of each interferometer therefore consisted of two "parallel" channels, which contain all information on total intensity (Stokes parameter I) and two "orthogonal" channels, which together with the parallel channels contain the polarization information (Stokes parameters Q, U and V).

Realizing that the signal to noise ratios for Q, U and V are (for almost all sources) too low to derive useful polarization information, we decided not to use the orthogonal channels, thereby considerably reducing the time required for the Fourier inversions. If desired, it is still possible to obtain polarization information because we did calibrate the orthogonal interferometer channels.

Before the start of the survey the pointing accuracy (at the declination of the survey) of all twelve telescopes was improved to about 0.02 degrees. As a result the antenna pattern of the twenty interferometers (and therefore of the telescope) is slightly wider than it was

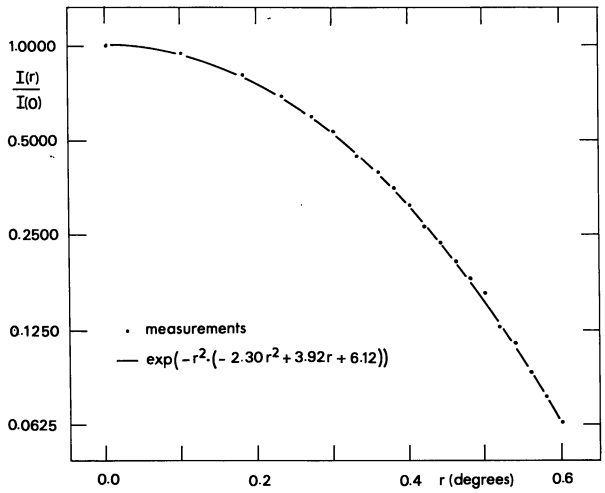

Fig. 1. The attenuation due to the primary beam pattern of the telescope. Dots indicate measured values, averaged over 40 interferometer channels and over all position angles. The line indicates the function that was used in correcting the attenuated flux densities to real-sky flux densities

during the first 1415 MHz survey (Katgert *et al.*, 1973). The antenna pattern of the telescope was measured by observing the sources 3C48 and 3C147 off-axis. More than sixty points in the sensitivity pattern were measured, out to a radial distance of 0.6 degrees and in several position angles. We found no evidence for deviations from circular symmetry. The average attenuation function is shown in Fig. 1. The analytic expression (a Gaussian with slowly varying dispersion) fits the data with an average quality of 1.2%, excluding the point at 0.5 degrees which deviates by 6.2%. This deviation is most probably due to an intrinsic property of the telescopes, and its reality has been confirmed by independent measurements.

Every day at least two calibration observations were done of fifteen minutes or more. From these observations we derived, for each day, gain corrections (mainly from 3C48) and instrumental phases (mainly from 3C295 which has a declination close to that of the survey). Occasional long runs on both calibrator sources were used to check the corrections of the twenty interferometer baselines with respect to a perfect East-West baseline. In order to ensure maximum consistency in the calibrations, we used one set of baseline parameters throughout the period.

The accuracy of the gain corrections is about 1.5% (per channel per day). The instrumental phases have an estimated accuracy of 2 degrees, while the baseline corrections are estimated to be accurate to within 2 millimeters (in length and orientation). The assumed positions and flux densities of the calibrator sources are:

	α(1950.0)	δ(1950.0)	S1415
3C 48	$1^h34^m49^s.83$	32°54′20″.8	15.67 f u
3C295	$14^h\ 9^m33^s.44$	52°26′13″.7	21.7 f.u.

Occasionally we observed the calibrator sources with a different dipole setting, i.e. with a relative position angle of 45 degrees between the dipoles in the movable and fixed telescopes. From these observations we determined the relative gains and phases of the forty orthogonal interferometer channels.

III. Fourier Transforms and First Stages of Data Analysis

The Fourier transform programme which, from the observed two-dimensional complex visibility function, produces a map of the sky brightness distribution is based on a fast Fourier transform algorithm due to Cooley and Tukey. For a detailed description of the programme we refer to Brouw (1971).

The actual properties of a map (and of the theoretical synthesized antenna pattern) can be specified by the user of the programme. One important property of all the maps that we made is that the number of synthesized intensities per half-power beamwidth is the same in right ascension and declination direction. This means that the synthesized antenna pattern is circular with respect to the two-dimensional grid of synthesized intensities. Also, the dimensions of all maps are identical, namely 1.5 degrees in right ascension and 1.5 cosec δ_o in declination direction.

In producing a map one can specify the relative weights to be given to the complex visibilities at the different baselines. These weights (or rather their distribution) determine the width and the shape of the synthesized antenna pattern and, at the same time, affect the noise per beam in the maps produced. By choosing the proper weight function it is possible, for instance, to produce maps with a minimum noise per beam. Unfortunately, the corresponding synthesized antenna pattern differs significantly from zero between the grating ellipses, and therefore is not very suitable for survey work.

For the observations of the present survey we used two sets of weight functions (grading functions). Firstly, we made high-resolution maps by applying weights that are proportional to baseline length, and which consequently compensate the relatively lower sampling density at the longer baselines. With this grading function, the weight per unit area in the aperture plane is constant. A cross-cut (in right ascension direction) through the resulting synthesized antenna pattern is shown in Fig. 2a. The half-power beamwidth is 22″ in right ascension direction and 22″ cosec δ_o in declination direction. For the purpose of combining our 1415 MHz data with the 408 MHz 5C2 data these high-resolution maps certainly are not ideal, because the large difference in beam solid angle will lead to a systematic underestimation of spectral indices of extended sources (the solid angle of the 5C2 beam is about thirteen times larger than that of our high-resolution beam).

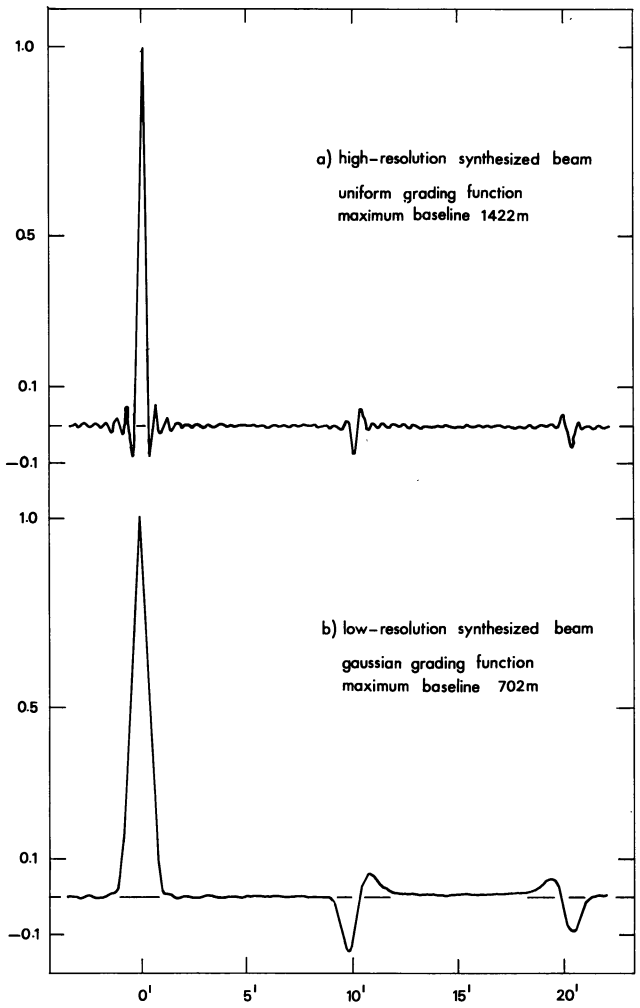

Fig. 2. Cross-cuts (in right ascension) through the two synthesized antenna patterns

We therefore also made low-resolution maps, in which all baselines larger than 702 m (3311 λ) were given zero weight. In addition to the weights that are proportional to baseline length we applied a Gaussian grading function with a value of 0.072 at the maximum baseline of 702 m. A cross-cut through the resulting synthesized antenna pattern is shown in Fig. 2b. It will be seen that this low-resolution beam has quite small inner sidelobes which is of great advantage for the determination of the integrated flux density of extended sources.

The differences between the high- and low-resolution maps may be summarized as follows:

a) the ratio of the half-power beamwidths is 2.65 but, due to the difference in beam shape, the ratio between the effective beamwidths is 3.2 (cf. Section IV)

b) assuming the noise figures of the twelve receivers to be identical, one finds that, theoretically, the noise per synthesized beam should be a factor 1.24 larger in the low-resolution maps than it is in the high-resolution maps

c) the correlation between adjacent synthesized intensities in the low-resolution maps is larger than in the

high-resolution maps due to a relatively higher sampling density per beam area

d) in the low-resolution maps confusion contributes relatively more to the errors in the flux density estimates than it does in the high-resolution maps.

Originally, the reason for making the low-resolution maps was to minimize an observational bias that affects the combination of the 5C2 data with our data. However, the low-resolution maps serve another purpose. In combination with the high-resolution maps, they enable us to determine total flux density and angular extent more consistently and with higher reliability than was possible in the first 1415 MHz survey. In Section IV we will discuss in more detail how we actually determined total flux densities and angular extent.

From every observation (i.e. for each of the twenty-four fields) we made four maps, viz. two high-resolution and two low-resolution maps. In addition to the two maps made direct from the observations, we also made maps from which all sources with an attenuated flux density larger than 20 m.f.u. were subtracted.

All ninety-six maps were analyzed by means of a source finding programme. This programme searches the map for all intensities that exceed a specified level. For the fifty strongest "possible" sources an iterative least squares fitting with the central part of the theoretical synthesized antenna pattern is done. This fitting procedure simultaneously determines the position and intensity of possible sources. The intensity levels defining such possible sources were set at 3.0 m.f.u. for all high-resolution maps and at 4.5 m.f.u. for all low-resolution maps.

For all twenty-four fields we combined the results of the four maps into one list of all possible sources with $\overline{S}_h \geqq 5.5$ m.f.u. and/or $\overline{S}_l \geqq 8.8$ m.f.u. ($\overline{S}_h$ and $\overline{S}_l$ denote *estimates* of attenuated flux density in the high- and low-resolution maps respectively). All possible sources in these twenty-four lists were finally inspected on contour plots, either of small parts of the original maps (subtracted sources) or of the complete subtract maps (all other sources). This inspection enabled us to determine which of the sources most probably were not real. At the same time we measured position angles of sources that, on the contour plots, appeared to be extended.

As a last step, we defined for every field a sample containing all real sources with $\overline{S}_h \geqq 6.25$ and/or $\overline{S}_l \geqq 10.75$ m.f.u. It should be stressed that these samples are complete (to the above limits) with respect to *estimated* attenuated flux density, as opposed to *real* attenuated flux density. Real sources with flux densities below the completeness limits have not been included in these samples because, firstly, they have little or no value for statistical work and secondly, the two deep fields will provide much better information about sources below the present completeness limits.

All sources that are considered to be positive detections of 5C2 sources, but which have estimated flux densities below the completeness limits have been entered in a separate list (cf. Section VII).

IV. Source Definition and Source Parameters

IVa. Source Definition

Before giving a description of how we determined source parameters, it is essential to discuss the source definition that we used. Ideally, one would like to be able to give a physically relevant definition of what constitutes a source. Unfortunately such a physical definition cannot be based on radio data alone. At best it can be based on combined radio and optical observations.

Because optical identification work on complete samples of weak radio sources so far yields identification percentages of at most 50%, one cannot but use source definitions that are based solely on radio observational criteria. Although such purely observational definitions are instrument- and frequency-dependent, they are statistically more relevant than definitions based partly on optical data (if available) and partly on radio data.

Observational source definitions are, generally, based on a predefined solid angle. An intensity distribution with a characteristic scale less than or not much larger than the scale of the predefined solid angle is then loosely defined as a source. In an attempt to base the source definition on a resolution criterion we used an analogy of the classical Rayleigh criterion. Our source definition is therefore based on the *absence of a relative minimum* in the intensity distribution. Taking into account the contour values used in the contour plots, such a relative minimum can have been detected only when its intensity is less than about 75% of the maximum intensity (this is an average value, for individual sources this value ranges from about 65% for the weakest sources to about 90% for the strongest sources).

This criterion was applied to the data from the low-resolution maps, for the following reasons. Firstly, the data from the low-resolution maps cannot be used when the source definition is based on the high-resolution data. Secondly, the source definition based on the low-resolution data is, for all practical purposes, identical to the one used for the 5C2 data (a notable exception being 5C2.50).

For accurate statistical work involving radio observations at several frequencies, one should obviously try to obtain observations made with more or less frequency-scaled aerials, in order to have the same source definition at the different frequencies. The difficulties that result from radically different source definitions (for instance in spectral index work) are illustrated in Table 2.

IVb. Source Positions

The source finding programme provides position estimates as well as errors in these estimates. These errors are based on the differences between the scaled syn-

Table 2. Differences in source definition

Source	(1)	(2)	(3)
1	1054+51W2	5C2.47	GB1054+51.4
2	1054+51W3	5C2.48	
3	1054+51W4		
4	1054+51W5	5C2.50	
5	1054+51W6		

(1): present paper
(2): Pooley and Kenderdine, 1968
(3): Maslowski, 1972

thesized antenna pattern and the observed intensities. However, they have not been corrected for the correlation between adjacent synthesized intensities. Consequently, the errors given by the source finding programme are too small by a constant factor which, in first order, depends on the sampling density (number of synthesized intensities per beam area). Because the sampling density is not the same in the high- and low-resolution maps, the position errors in the two types of map have not necessarily been underestimated by the same factor.

Yet, analysis of the ratio of high- and low-resolution position errors, as given by the source finding programme, shows that the average position error ratio is equal to the ratio of the effective beamwidths. This must be caused by the different shapes of the two synthesized antenna patterns (i.e. by the different forms of the two correlation functions). For this reason we have assumed that source finding programme position errors in high- and low-resolution maps are too small by the same factor.

About one third of all sources was detected in only either the high-resolution or low-resolution map. For the remaining two thirds we have two estimates of the source position. Considering the totally different weighting of the complex visibility functions in the two types of map, these two position estimates are almost completely independent. From these two position estimates we therefore made a weighted average, with weights that are inversely proportional to the squares of the source finding programme errors. The error in the average position estimate was derived from the two errors, assuming complete independence of the two estimates.

About thirty sources were detected in more than one field. Analysis of their positions in the different fields served to determine the constant factor by which all position errors yielded by the source finding programme should be multiplied. After multiplication of the errors by 1.3, seventy per cent of the position differences were less than their combined errors. The position errors in the source list (which have all been corrected accordingly) can therefore be considered to represent mean error estimates.

The internal consistency of the positional systems in the different fields is estimated to be better than 0.3 s of arc. Those position errors that, formally, are smaller than 0.3 s of arc were consequently set equal to this limiting value. Finally, it is estimated that the positional system of the present survey agrees to within 0.3 s of arc with the system defined by the sources 3C48 and 3C295.

IV c. Flux Densities

The determination of the flux densities is slightly more complicated than the determination of the positions. As with the positions, we have for about two thirds of the sources two almost completely independent attenuated flux density estimates, viz. $\bar{S}_h$ and $\bar{S}_l$. In principle, these two flux density estimates together contain information on the gross characteristics of the intensity distribution of a source.

Such characteristics can only be quantified on the assumption of a specific model of the intensity distribution. The simplest possible model is that of an equal double source, characterized by the following parameters: a) total flux density and b) separation between the two (equal) components. It is clear that the majority of the sources can, in reality, not be fitted in such a simple model. One obvious improvement with respect to the equal double source model would be the introduction of unequal components. However, one must have a rather detailed knowledge of the distribution function of component flux density ratios in order to improve drastically on the equal double source model.

We therefore decided to use this equal double source model, and calibrated the effects of the high- and low-resolution synthesized beams on the flux density of equal double sources with known separation and total flux density. To this end we injected such well-defined equal double sources into an artificial map. We found the following relations:

$$\bar{S}_t^* = \bar{S}_h^{*\,-0.108} \cdot \bar{S}_l^{*\,1.108} \tag{1}$$

and

$$\Psi_{eq}^* = 28.65\,(\ln(\bar{S}_l^*/\bar{S}_h^*))^{\frac{1}{2}} \tag{2}$$

where $\bar{S}_t^*$, $\bar{S}_h^*$ and $\bar{S}_l^*$ denote *real* (noise-free) total, high- and low-resolution flux densities respectively, while Ψ_{eq}^* denotes the real separation (in seconds of arc) between the two components. Due to the ellipticity of the synthesized antenna pattern, this equivalent separation is related to the actual separation Ψ^* by:

$$\Psi_{eq}^* = \Psi^*(1 - \cos^2\phi\cos^2\delta)^{\frac{1}{2}} \tag{3}$$

where ϕ denotes the position angle (from north through east) of the line joining the two components.

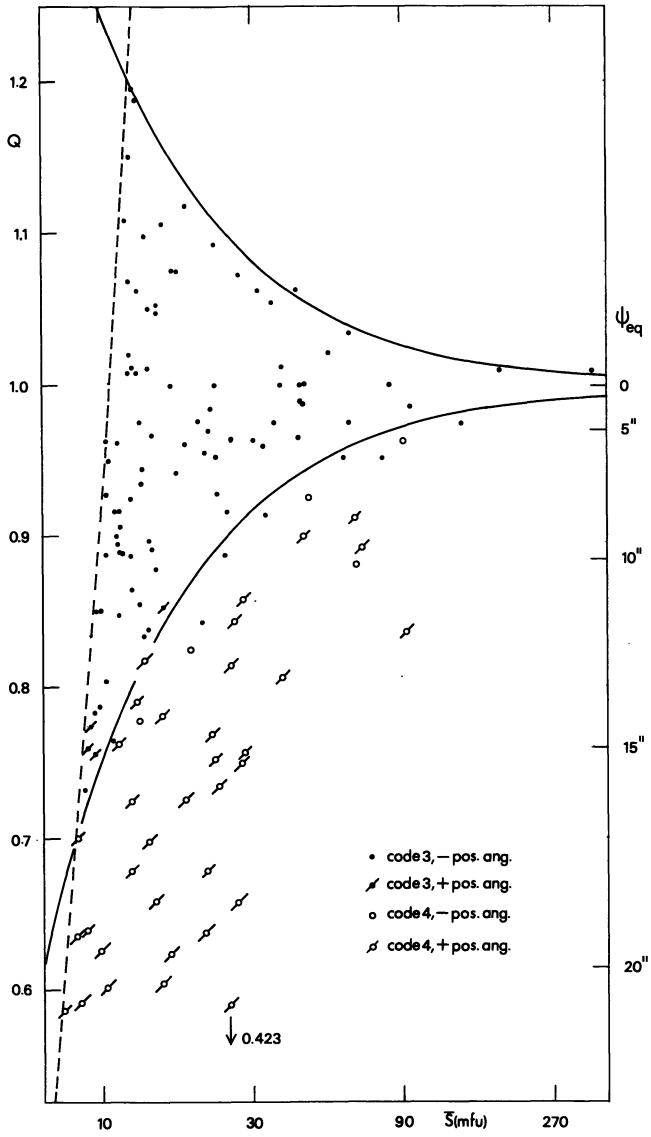

Fig. 3. The distribution of $Q(=\bar{S}_h/\bar{S}_l)$ with respect to $\bar{S}$ (the weighted average of $\bar{S}_h$ and $\bar{S}_l$). Dots and circles indicate sources that were defined non-extended (Code 3) and extended (Code 4) respectively. Sources for which a position angle could be determined on the contour plots have been marked. For an explanation of the meaning of the dashed and solid lines we refer to the text (Section IVc). On the right hand side Ψ_{eq} is shown

The above relations hold for the *real* parameters, while we only have *estimates* of the two flux densities (and the errors in these estimates) at our disposal. For this reason we can use the above relations only for sources that have a high probability of being really extended. The first question to be answered is therefore when a source should be considered extended. In other words: given $\bar{S}_h$ and $\bar{S}_l$ with their respective errors $\Delta\bar{S}_h$ and $\Delta\bar{S}_l$, what is the probability that $\bar{S}_h$ and $\bar{S}_l$ are actually estimates of the same total flux density $\bar{S}_t^*$. Having answered this question one should decide at what level of probability a source will be considered to be extended.

One way to approach this problem is by considering the parameter $Q^* \equiv \bar{S}_h^*/\bar{S}_l^*$ (which is explicitly present in the formula for Ψ_{eq}^* and implicitly in the formula for $\bar{S}_t^*$). Obviously, Q^* is unity for non-extended (point-) sources and less than unity for extended sources. Q, i.e. the estimated value of Q^*, may differ substantially from unity even for non-extended sources.

The problem then becomes one of defining $Q_{\min}(\bar{S}_t^*)$, i.e. the value of Q below which a source will be *defined* as extended. In principle, one needs the distribution function of Q for non-extended sources in order to compute the probability level associated with a given $Q_{\min}(\bar{S}_t^*)$ or, vice versa, to compute $Q_{\min}(\bar{S}_t^*)$ given a certain probability level. It can be shown that, on the assumption of normally distributed errors in the estimates $\bar{S}_h$ and $\bar{S}_l$, the distribution of Q (for non-extended sources) is very nearly identical to a normal distribution function with variance $(\Delta\bar{S}_h^2 + \Delta\bar{S}_l^2)/\bar{S}_t^{*2}$, provided that $\bar{S}_t^*$ is sufficiently large. In that case, the probability of a non-extended source having a Q-value less than $1-(\Delta\bar{S}_h^2 + \Delta\bar{S}_l^2)^{\frac{1}{2}}/\bar{S}_t^*$ is less than 16%.

In Fig. 3 we have plotted Q against $\bar{S}_t$ for all sources with $\bar{S}_h \geqq 6.25$ m.f.u. and $\bar{S}_l \geqq 10.75$ m.f.u. For $\bar{S}_t$ we used the weighted average of $\bar{S}_h$ and $\bar{S}_l$ (with weights inversely proportional to $\Delta\bar{S}_h^2$ and $\Delta\bar{S}_l^2$), i.e. assuming $\bar{S}_h$ and $\bar{S}_l$ to be independent estimates of the same $\bar{S}_t^*$. The solid curves represent

$$Q = 1 \pm (\Delta\bar{S}_h^2 + \Delta\bar{S}_l^2)^{\frac{1}{2}}/\bar{S}_t$$

for $\Delta\bar{S}_h = 1.25$ m.f.u. and $\Delta\bar{S}_l = 2.15$ m.f.u., while the almost vertical line on the left hand side represents $Q(\bar{S}_t)$ for $\bar{S}_l = 10.75$ m.f.u.

Filled and open circles denote sources for which Q is larger (Code 3) or smaller (Code 4) than $1-(\Delta\bar{S}_h^2 + \Delta\bar{S}_l^2)^{\frac{1}{2}}/\bar{S}_t$ respectively, while sources for which we could determine a position angle from the contour plots have been indicated. On the basis of Fig. 3 we conclude that the distinction between sources of Classes 3 and 4 corresponds satisfactorily with the distinction on the basis of detectability of a position angle. For this reason we have adopted the following criterion for *defining* extended sources: every source for which $Q < Q_{\min}(\bar{S}_t)$ [where $Q_{\min}(\bar{S}_t) = 1-(\Delta\bar{S}_h^2 + \Delta\bar{S}_l^2)^{\frac{1}{2}}/\bar{S}_t$] was *defined* to be extended (Code 4 in Fig. 3), irrespective of the detectability of a position angle. On the other hand, every source with $Q > Q_{\min}(\bar{S}_t)$ was defined to be non-extended (Code 3 in Fig. 3), again irrespective of its appearance on the contour plots.

The probability level associated with this particular choice of $Q_{\min}(\bar{S}_t)$ was evaluated numerically. In Table 3 we have listed the probability that an ideal point source with flux density $\bar{S}^*$ has incorrectly been defined as extended, with the definition based on the above criterion.

Table 3. Probability of incorrectly defining a point source to be extended

$\bar{S}^*$ (m.f.u.)	P(%)
10.8	11
14.0	12
19.0	13
26.5	14
45.0	15
>100	16

The attenuated flux densities of sources detected in both types of map were derived as follows:
a) for sources defined non-extended (Code 3) the flux density is the weighted average of $\bar{S}_h$ and $\bar{S}_l$, i.e.

$$\bar{S} = (\bar{S}_h \Delta\bar{S}_l^2 + \bar{S}_l \Delta\bar{S}_h^2)/(\Delta\bar{S}_h^2 + \Delta\bar{S}_l^2)\,. \quad (4)$$

b) for sources defined extended (Code 4) we computed the flux density by using Eq. (1), i.e.

$$\bar{S} = \bar{S}_h^{-0.108}\bar{S}_l^{1.108} = \bar{S}_h Q^{-1.108} = \bar{S}_l Q^{-0.108} \quad (5)$$

Eq. (5) is, strictly speaking, only valid for equal double sources. Using this relation also for more realistic (and therefore more complicated) source structures causes, in general, $\bar{S}$ to be slightly overestimated. This overestimation amounts to at most 6% for sources with an equivalent diameter of 22 s of arc.
The flux densities of sources detected only in either the high-resolution map (Code 1) or the low-resolution map (Code 2) were simply set equal to $\bar{S}_h$ or $\bar{S}_l$. Flux densities of sources detected only in the low-resolution map, but for which we could estimate an angular extent, were corrected by means of Eq. (5) in combination with Eq. (2) [i.e. $\bar{S} = \bar{S}_l \exp((\Psi_{eq}/87.2)^2)$].
For the determination of the actual flux density errors we did not use the errors given by the source finding programme. Instead we determined the actual noise in the maps by analyzing the distribution of possible sources with respect to flux density (a more detailed discussion will be given in Paper III). We found values of 1.25 and 2.15 m.f.u. for the average noise per synthesized beam in the twenty-four high-and low-resolution maps respectively. The ratio of these values differs from what one expects theoretically (cf. Section III), probably because confusion noise is not negligible in the low-resolution maps.
The flux density errors $\Delta\bar{S}_h$ and $\Delta\bar{S}_l$ were consequently set equal to 1.25 and 2.15 m.f.u. unless there was an obvious reason for increasing one or both of the errors (such as: complex structure of a source or, for the stronger sources, the domination of the uncertainty in the gain corrections (cf. Section II) over the random errors in the flux density determination). For sources with Codes 3 or 4 we computed the error in the flux density from $\Delta\bar{S}_h$ and $\Delta\bar{S}_l$, assuming $\bar{S}_h$ and $\bar{S}_l$ to be completely independent.
The final correction, applied to the flux density of all sources, is the correction for the attenuation due to the antenna pattern of the telescope. After multiplication by the attenuation factor, the error in the (real sky) flux density contains a contribution due to the uncertainty in the attenuation factor. This contribution is, for almost all sources, small compared with the error in the flux density estimate.
Analysis of the differences in the real sky flux densities of sources detected in more than one map shows that the final flux density errors (i.e. those given in the source list, cf. Table 4) represent mean errors.

IV d. Source Structure

There are two kinds of sources for which structure could be detected. Firstly, there are sources with an equivalent separation less than about 22 s of arc (i.e. sources not completely resolved by the high-resolution beam, but which have been defined extended due to a sufficiently large signal to noise ratio). For these sources we used Eqs. (2) and (3) to compute the actual equivalent separation. If a position angle had been determined from the contour plots, this position angle was used in Eq. (3). On the other hand, when no position angle was available we applied an average factor Ψ^*/Ψ^*_{eq} based on an isotropic distribution of the position angles.
It should again be stressed that Eq. (2) is correct for equal double sources only. Consequently the actual separation of more complicated structures may be considerably larger than the equivalent separation computed from Eq. (2). Therefore one should be very careful in using the quoted separations for statistical purposes.
The second kind of source for which structure could be detected is that of the complex sources (Code 5). For these sources the intensity distribution was either clearly resolved into two or more components or could, without ambiguity, be decomposed into several components. For these complex sources we have given an overall position angle and, in most cases, a contour plot. These contour plots are shown in Fig. 4.
The estimated accuracy of the quoted position angles (which have been rounded off to the nearest multiple of 5 degrees) is of the order of 10 degrees.

V. Source List

The source list (cf. Table 4) gives all relevant information about the detected sources. Only those sources have been listed that have a primary beam attenuation factor of less than 10. This corresponds to a maximum radius of the circular search area (for each field) of 0.551 degrees.
Care has been taken to allow sufficiently accurate recovery of all original flux density information. The relevant relations are given at the end of this section.

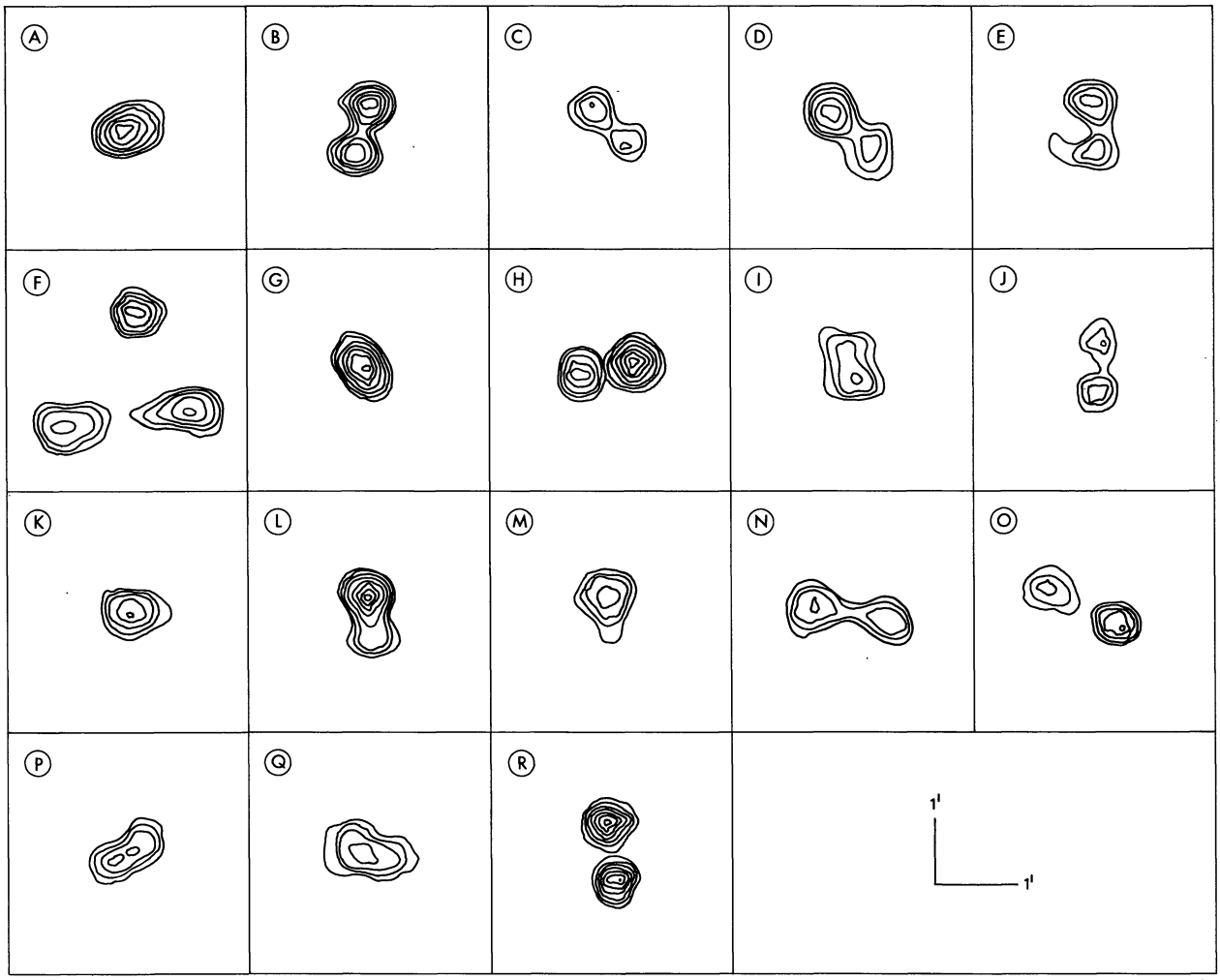

Fig. 4A–R. Contour plots (from the high-resolution maps) of sixteen complex sources. The declination scale has been compressed by a factor $\sin\delta$ in order to make the synthesized beam circular. As a result, position angles in the contour plots do not correspond to real-sky position angles. Lowest contours have values between 1.4 and 2.4 times the noise. The sources are: (A) 1048 + 51W3*, (B) 1050 + 47W1*, (C) 1054 + 48W3* (field 4), (D) 1054 + 48W3* (field 5), (E) 1054 + 49W1*, (F) 1054 + 51W4, 5 and 6, (G) 1059 + 48W1*, (H) 1100 + 51W1*, (I) 1101 + 47W3, (J) 1101 + 48W1*, (K) 1102 + 47W2*, (L) 1108 + 49W1* (field 22), (M) 1108 + 49W1* (field 20), (N) 1109 + 48W1*, (O) 1109 + 49W4*, (P) 1109 + 50W1, (Q) 1111 + 48W2, (R) 1111 + 51W1*

The organization of Table 4 is as follows:

Column 1: the name of the source in a modified Parkes system (cf. Katgert *et al.*, 1973). Complex sources have been given one name followed by an asterisk. The components (which need not be physically related) have been given the same name followed by the letters *A*, *B* etc.

Column 2: right ascension (epoch 1950.0) and its mean error (cf. Section IV b)

Column 3: declination (epoch 1950.0) and its mean error (cf. Section IV b)

Column 4: primary beam attenuation factor (cf. Section II)

Column 5: real sky 1415 MHz flux density and its mean error (cf. Section IV c)

Column 6: flux density code with the following meaning:

1. detected only in high-resolution map
2. detected only in low-resolution map
3. detected in both maps; non-extended (cf. Section IV c)
4. detected in both maps; extended (cf. Section IV c)
5. complex source (cf. Section IV d)

Column 7: Q i.e. the ratio of $\bar{S}_h$ and $\bar{S}_l$ (cf. Section IV c)

Column 8: Q_e i.e. the ratio of $\Delta\bar{S}_h$ and $\Delta\bar{S}_l$

Column 9: Ψ i.e. the actual equivalent separation in seconds of arc (cf. Section IV d)

Column 10: ϕ i.e. the position angle of the "major axis" of the intensity distribution (from north through east)

Column 11: 5C2 number (cf. Pooley and Kenderdine, 1968)

Column 12: references to contour plots and additional remarks.

The original flux density information may be obtained by using the following relations (S and ΔS refer to the parameters given in Column 5 *divided* by the attenuation factor).

Code 1	$\bar{S}_h = S$	$\Delta\bar{S}_h \sim \Delta S$
Code 2	$\bar{S}_l = S$	$\Delta\bar{S}_l \sim \Delta S$
Code 3	$\bar{S}_h = S \cdot Q \cdot (1+Q_e^2)/(Q+Q_e^2)$	$\Delta\bar{S}_h \sim \Delta S \cdot (1+Q_e^2)^{\frac{1}{2}}$
	$\bar{S}_l = S \cdot (1+Q_e^2)/(Q+Q_e^2)$	$\Delta\bar{S}_l \sim \Delta S \cdot (1+Q_e^2)^{\frac{1}{2}}/Q_e$
Code 4	$\bar{S}_h = S \cdot Q^{1.108}$	$\Delta\bar{S}_h \sim 0.9\,\Delta S \cdot Q_e \cdot Q^{0.108}$
	$\bar{S}_l = S \cdot Q^{0.108}$	$\Delta\bar{S}_l \sim 0.9\,\Delta S \cdot Q^{0.108}$
Code 5	use relations for Codes 1 and 2	

1975A&A....38...87K

Table 4. Source list

NAME	RA(1950.0)	DEC(1950.0)	ATTEN	S1415(MFU)	SCODE	Q	QE	PSI	PHI	5C2.	REMARKS
1048+47W1	10 48 8.70 ± 0.06	47 58 1.4 ± 0.7	6.259	77.1 ± 6.8	3	1.008	0.58				
1048+47W2	10 48 32.39 0.09	47 48 36.9 1.1	4.714	95.0 5.5	3	0.976	0.65			2	
1048+50W1	10 48 5.57 0.12	50 58 12.0 1.4	2.040	19.5 2.2	3	0.756	0.58		135		
1048+51W1	10 48 41.17 0.11	51 9 46.6 1.0	1.910	47.6 2.8	3	0.887	0.94			4	
1048+51W2	10 48 46.88 0.19	51 2 18.2 2.4	1.405	11.5 1.8	1						
1048+51W3*	10 48 55.90 0.12	51 7 46.4 1.5	1.551	73.7 3.3	5				115	5	CNT
1048+51W3A	10 48 54.01 0.31	51 7 57.0 3.9	1.584	14.2 3.2	1						
1048+51W3B	10 48 56.09 0.17	51 7 46.2 1.9	1.549	48.8 3.9	1						
1048+51W3C	10 48 58.16 0.34	51 7 36.6 4.2	1.517	10.6 2.3	1						
1049+47W1	10 49 30.29 0.06	47 50 17.6 0.7	1.864	42.9 2.3	3	1.000	0.67				
1049+48W1	10 49 21.09 0.07	48 53 5.4 0.9	5.487	205.8 6.8	3	1.000	0.70			7	
1049+48W2	10 49 29.54 0.07	48 3 5.9 0.9	1.751	25.7 1.9	3	0.891	0.58				
1049+48W3	10 49 39.37 0.35	48 55 53.6 4.6	3.481	23.0 5.2	1					10	
1049+48W4	10 49 48.37 0.06	48 20 28.0 0.8	3.971	58.1 4.3	3	0.967	0.58			12	
1049+48W5	10 49 56.94 0.10	48 42 32.1 1.4	7.127	120.4 7.7	3	1.075	0.58			13	
1049+49W1	10 49 32.83 0.12	49 45 57.2 1.6	1.688	12.1 2.1	1				65	8	
1049+49W2	10 49 39.15 0.11	49 53 14.0 1.4	1.219	11.2 1.3	3	0.774	0.58		110	9	
1049+50W1	10 49 0.92 0.06	50 58 24.1 0.7	1.218	17.4 1.3	3	0.897	0.58				
1049+50W2	10 49 41.18 0.10	50 43 38.3 1.1	1.491	23.5 1.6	3	1.106	0.58			11	
1049+51W1	10 49 36.29 0.14	51 21 35.7 1.7	3.414	25.1 4.3	1						
1050+47W1*	10 50 55.61 0.22	47 37 2.0 2.9	2.428	139.6 10.9	5				165	17	CNT
1050+47W1A	10 50 55.06 0.24	47 37 24.0 3.2	2.352	64.7 5.9	1						
1050+47W1B	10 50 55.36 0.17	47 36 56.8 2.4	2.447	18.3 3.7	1						
1050+47W1C	10 50 56.10 0.22	47 36 36.4 3.0	2.521	56.7 6.3	1						
1050+49W1	10 50 47.44 0.03	49 45 54.3 0.4	1.447	70.3 3.5	4	0.901	0.58	9	90	16	
1050+50W1	10 50 23.27 0.02	50 5 22.3 0.3	1.066	45.5 1.1	3	0.965	0.58			14	
1050+51W1	10 50 14.66 0.09	51 22 4.0 1.0	3.437	51.8 3.7	3	1.052	0.58				
1050+51W2	10 50 26.80 0.04	51 15 36.9 0.4	1.952	83.9 2.6	3	1.000	0.50			15	
1050+51W3	10 50 38.24 0.15	51 2 21.4 1.8	1.094	7.9 1.4	1						
1050+51W4	10 50 47.04 0.06	51 7 18.1 0.7	1.297	14.9 1.4	3	0.899	0.58				
1051+47W1	10 51 0.09 0.08	47 59 18.6 1.1	1.005	12.7 1.1	3	1.195	0.58				
1051+47W2	10 51 42.04 0.40	47 48 22.4 5.3	1.276	13.9 2.7	2						
1051+49W1	10 51 2.88 0.13	49 55 31.4 1.7	1.083	9.0 1.3	1					18	
1051+50W1	10 51 24.82 0.02	50 51 23.1 0.3	1.444	77.1 1.6	3	1.022	0.58			19	
1051+50W2*	10 51 40.69 0.38	50 3 46.4 4.7	1.321	15.7 2.8	5				55	21	
1051+50W2A	10 51 38.24 0.41	50 3 27.4 5.2	1.292	7.0 1.6	1						
1051+50W2B	10 51 41.99 0.23	50 3 51.1 2.9	1.336	9.1 1.7	1						
1051+50W3	10 51 57.46 0.11	50 3 48.6 1.3	1.516	12.8 1.9	1						
1051+51W1	10 51 9.80 0.22	51 14 30.2 2.7	2.170	13.9 2.7	1						
1051+51W2	10 51 26.28 0.15	51 14 15.2 1.8	2.412	15.9 3.0	1						
1052+48W1	10 52 12.64 0.12	48 53 38.9 1.6	1.353	10.4 1.7	1					25	
1052+48W2	10 52 13.60 0.06	48 13 15.5 0.9	2.041	21.4 2.5	1						
1052+48W3	10 52 38.93 0.14	48 2 52.1 1.8	1.677	11.1 2.1	1						

1975A&A....38...87K

Table 4 (continued)

NAME	RA(1950.0)	DEC(1950.0)	ATTEN	S1415(MFU)	SCODE	Q	QE	PSI	PHI	5C2.	REMARKS
1052+49W1	10 52 13.21 ± 0.09	49 49 49.6 ±1.0	2.082	19.6 ± 2.6	1					26	
1052+50W1	10 52 2.84 0.17	50 54 1.9 2.1	2.002	16.2 2.5	1						
1053+48W1	10 53 29.12 0.11	48 42 55.2 1.4	1.887	26.2 4.6	4	0.763	0.70	17	30	29	
1053+48W2	10 53 49.10 0.06	48 48 54.6 0.8	1.623	43.4 4.6	4	0.769	0.80	16	40	34	
1053+48W3	10 53 52.66 0.28	48 50 22.8 3.7	1.632	32.7 3.5	2				65		D=25"
1053+49W1	10 53 39.50 0.08	49 21 11.6 1.0	2.806	59.7 3.1	3	0.954	0.61			33	
1053+49W2	10 53 52.51 0.04	49 49 48.6 0.5	2.928	127.4 8.3	4	0.806	0.80	15	35	36	
1053+50W1	10 53 31.88 0.02	50 35 54.4 0.3	2.293	86.9 2.5	3	1.013	0.58			30	
1053+52W1	10 53 51.58 0.07	52 11 20.2 0.8	2.247	36.9 5.5	4	0.778	0.58	15			HALO?
1054+48W1	10 54 2.80 0.11	48 32 39.7 1.5	1.663	12.4 2.1	1					38	
1054+48W2	10 54 7.58 0.03	48 52 47.6 0.4	1.561	52.3 2.1	3	0.914	0.50			39	
1054+48W3*	10 54 26.36 0.30	48 59 13.5 3.9	1.938	82.3 14.5	5				40	43	CNT
1054+48W3A	10 54 24.44 0.29	48 58 59.7 3.8	1.930	19.3 3.9	1						
1054+48W3B	10 54 27.01 0.13	48 59 27.1 1.6	1.961	47.0 4.9	1						
1054+48W4	10 54 38.84 0.12	48 12 53.2 1.5	7.273	208.6 21.1	4	0.678	0.72	17	75	46	
1054+49W1*	10 54 12.61 0.55	49 48 54.5 7.1	2.167	61.7 15.2	5				5	40	CNT
1054+49W1A	10 54 12.01 0.34	49 48 20.1 4.2	2.140	21.4 5.4	1						RESOLVED
1054+49W1B	10 54 12.35 0.18	49 49 6.3 2.3	2.188	36.1 5.5	1						RESOLVED
1054+49W2	10 54 35.99 0.05	49 14 30.2 0.7	4.678	141.1 11.4	4	0.814	0.70	14	125	45	
1054+50W1	10 54 26.44 0.13	50 18 43.6 1.6	1.295	14.4 1.6	1					42	
1054+51W1	10 54 34.06 0.03	51 56 57.0 0.3	2.281	157.8 5.5	4	0.912	0.58	8	90	44	
1054+51W2	10 54 40.25 0.07	51 15 44.9 0.8	1.606	36.1 2.2	3	0.985	0.82			47	
1054+51W3	10 54 40.35 0.04	51 11 53.0 0.5	1.743	55.0 2.0	3	1.063	0.45			48	
1054+51W4	10 54 41.83 0.11	51 22 9.0 1.3	1.578	49.7 9.2	4	0.637	0.50	19	90	50	CNT
1054+51W5	10 54 46.00 0.06	51 23 37.0 0.7	1.553	32.3 2.1	3	0.842	0.43			50	CNT
1054+51W6	10 54 51.38 0.13	51 21 53.5 1.6	1.443	34.2 5.9	4	0.622	0.64	19	90	50	CNT
1055+47W1	10 55 57.37 0.44	47 43 43.3 6.0	2.301	25.8 4.9	2						
1055+48W1	10 55 10.22 0.08	48 42 15.1 1.2	1.004	12.0 1.1	3	0.889	0.58			55	
1055+49W1	10 55 17.71 0.03	49 55 40.4 0.4	1.741	242.4 5.0	3	0.975	1.00			56	
1055+49W2	10 55 25.99 0.07	49 29 38.8 0.9	1.339	110.4 4.5	3	1.000	0.90			59	
1055+49W3	10 55 53.57 0.12	49 31 17.2 1.5	1.176	15.8 1.3	3	0.974	0.58			62	
1055+50W1	10 55 8.66 0.15	50 39 30.6 1.7	1.435	17.9 3.6	4	0.639	0.70	23	25	53	
1055+50W2	10 55 8.78 0.07	50 44 16.4 0.9	1.956	26.8 2.7	3	1.096	0.81			54	
1055+50W3	10 55 25.56 0.09	50 7 14.1 1.1	2.007	43.9 5.1	4	0.604	0.81	20	65	58	
1055+50W4	10 55 40.26 0.26	50 45 26.5 3.1	2.148	14.6 3.2	1					61	
1055+51W1	10 55 10.97 0.12	51 36 19.1 1.4	2.260	18.0 2.8	1						
1055+51W2	10 55 17.80 0.02	51 37 56.1 0.3	2.446	144.5 2.8	3	0.952	0.45			57	
1055+51W3	10 55 25.83 0.10	51 21 43.1 1.2	1.146	12.1 1.2	3	0.887	0.58				
1055+51W4	10 55 32.27 0.11	51 26 0.9 1.3	1.205	11.2 1.5	1						
1055+51W5	10 55 35.87 0.20	51 57 27.7 2.4	1.556	23.8 3.9	4	0.600	0.70	20	65		
1055+51W6	10 55 36.62 0.03	51 22 45.6 0.3	1.107	33.9 1.2	3	0.963	0.58				
1055+51W7	10 55 39.19 0.19	51 51 25.9 2.1	2.396	23.6 2.9	3	0.787	0.70				
1055+51W8	10 55 45.33 0.09	51 3 38.7 1.2	1.666	18.7 1.8	3	0.917	0.58				
1055+52W1	10 55 2.76 0.49	52 11 22.6 5.8	1.172	14.6 2.5	2						
1055+52W2	10 55 26.66 0.66	52 11 45.5 7.9	1.057	12.7 2.3	2						
1055+52W3	10 55 27.17 0.06	52 8 17.0 0.6	1.083	18.9 1.2	3	1.076	0.58				

1975A&A....38...87K

Table 4 (continued)

NAME	RA(1950.0)	DEC(1950.0)	ATTEN	S1415(MFU)	SCODE	Q	QE	PSI	PHI	5C2.	REMARKS
1056+48W1	10 56 19.36 ± 0.06	48 3 11.8 ± 0.9	2.408	25.3 ± 2.6	3	0.928	0.58			66	
1056+48W2	10 56 51.17 0.14	48 25 5.5 1.9	3.106	20.8 4.7	1				90	72	
1056+48W3	10 56 53.20 0.11	48 20 41.1 1.4	4.666	56.4 11.7	4	0.635	0.58	19	90	73	
1056+49W1	10 56 59.72 0.10	49 42 32.4 1.2	1.178	38.2 3.1	4	0.757	1.23	15	120	74	
1056+50W1	10 56 6.26 0.03	50 31 1.9 0.4	1.139	28.8 1.2	3	0.917	0.58			64	
1056+50W2	10 56 20.10 0.02	50 22 49.8 0.3	1.182	41.2 1.3	3	1.055	0.58			67	
1056+51W1	10 56 16.25 0.02	51 12 50.9 0.3	1.071	200.0 1.5	3	1.011	0.80			65	
1056+51W2	10 56 27.49 0.06	51 34 46.8 0.7	1.629	23.0 1.8	3	0.837	0.60				
1056+52W1	10 56 0.08 0.18	52 24 4.8 2.1	1.319	11.0 1.6	1						
1056+52W2	10 56 18.05 0.02	52 26 31.3 0.3	1.517	183.3 2.0	1						
1057+48W1	10 57 11.28 0.05	48 3 19.7 0.6	1.600	27.8 1.7	3	0.942	0.58			75	
1057+49W1	10 57 14.96 0.10	49 56 27.9 1.2	2.171	25.4 2.3	3	0.890	0.58			77	
1057+49W2	10 57 41.15 0.12	49 36 31.3 1.5	1.687	15.8 2.1	1					79	
1057+50W1	10 57 33.44 0.12	50 30 42.6 1.4	2.446	19.2 3.1	1					78	
1057+51W1	10 57 2.96 0.06	51 10 17.9 0.8	1.266	11.4 1.4	3	0.759	0.58		90		
1057+51W2	10 57 11.30 0.17	51 13 43.7 2.0	1.199	7.8 1.8	1						
1057+52W1	10 57 41.43 0.02	52 52 27.1 0.3	8.392	510.9 10.3	3	0.974	0.70				
1058+47W1	10 58 5.18 0.04	47 45 10.5 0.5	1.040	19.2 1.1	3	1.118	0.58				
1058+47W2	10 58 25.51 0.15	47 45 27.4 2.0	1.084	8.1 1.3	1						
1058+47W3	10 58 37.76 0.10	47 41 0.6 1.4	1.268	11.0 1.6	1						
1058+47W4	10 58 41.14 0.07	47 52 40.3 0.9	1.143	14.5 1.2	3	1.012	0.58				
1058+47W5	10 58 59.39 0.08	47 45 27.7 1.2	1.295	23.8 3.2	4	0.698	0.70	19	40	92	
1058+48W1	10 58 30.81 0.08	48 4 44.1 1.1	1.693	19.3 1.8	3	0.848	0.58			87	
1058+48W2	10 58 58.46 0.05	48 57 4.7 0.7	2.631	57.2 2.8	3	0.958	0.58			91	
1058+49W1	10 58 24.34 0.14	49 40 30.0 1.8	2.879	24.0 3.6	1					85	
1058+49W2	10 56 32.69 0.06	49 6 38.9 0.7	1.526	45.1 3.7	4	0.843	0.94	13	150	88	
1058+51W1	10 58 31.28 0.07	51 14 41.3 0.8	2.481	28.4 2.7	3	0.962	0.58			86	
1058+52W1	10 58 7.36 0.05	52 6 46.2 0.6	2.178	68.7 5.3	4	0.858	0.82	13	175	82	
1058+52W2	10 58 16.70 0.36	52 17 16.5 4.1	2.448	28.5 6.2	4	0.591	0.93	21	50		
1058+52W3	10 58 18.62 0.05	52 32 12.1 0.5	3.736	131.0 10.7	4	0.748	0.60	16	135		
1058+52W4	10 58 41.63 0.17	52 13 10.8 1.9	3.339	20.9 4.2	1						
1059+47W1	10 59 7.32 0.09	47 48 31.4 1.2	1.335	14.3 1.4	3	0.950	0.58				
1059+47W2	10 59 18.52 0.12	47 45 28.5 1.6	1.522	13.3 2.3	1						
1059+47W3	10 59 20.49 0.07	47 49 5.9 1.0	1.501	19.6 1.6	3	1.183	0.58			97	
1059+48W1*	10 59 4.81 0.04	48 24 8.3 0.5	1.162	195.3 12.8	5				25	94	CNT
1059+48W1A	10 59 3.80 0.19	48 23 46.9 2.6	1.178	32.4 5.9	1						
1059+48W1B	10 59 4.80 0.10	48 24 8.3 1.3	1.162	134.3 8.7	1						
1059+48W1C	10 59 5.79 0.31	48 24 28.6 4.1	1.148	28.7 7.5	1						
1059+48W2	10 59 37.31 0.13	48 3 37.6 1.7	2.735	36.8 6.9	4	0.625	0.81	19	95	99	
1059+48W3	10 59 58.96 0.12	48 20 10.9 1.7	1.521	24.1 1.6	3	0.851	0.58		30	104	
1059+50W1	10 59 32.62 0.20	50 59 31.8 2.3	1.239	13.6 1.5	1						
1059+53W1	10 59 53.65 0.19	53 6 20.6 2.2	4.784	34.2 6.0	1						
1100+49W1	11 0 49.25 0.08	49 22 52.7 1.0	1.465	16.6 1.6	3	0.917	0.58			110	
1100+51W1*	11 0 49.50 0.22	51 10 13.6 2.7	2.362	273.9 19.0	5				115	109	CNT
1100+51W1A	11 0 48.04 0.13	51 10 18.5 1.5	2.363	153.6 14.2	1						
1100+51W1B	11 0 50.11 0.17	51 10 11.4 1.8	2.360	20.1 3.5	1						

Table 4 (continued)

NAME	RA(1950.0)	DEC(1950.0)	ATTEN	S1415(MFU)	SCODE	Q	QE	PSI	PHI	5C2.	REMARKS
1100+51W1C	11 0 52.26 ± 0.15	51 10 7.0 ± 1.9	2.368	100.6±11.8	1						
1100+52W1	11 0 13.70 0.12	52 41 54.5 1.3	1.083	8.6 1.4	1						
1101+47W1	11 1 0.28 0.07	47 16 12.7 0.9	1.457	15.3 1.6	3	0.963	0.58				
1101+47W2	11 1 42.14 0.20	47 23 36.9 2.8	1.038	6.6 1.4	1						
1101+47W3	11 1 52.14 0.45	47 43 3.0 6.1	2.087	68.6 10.4	2				170	126	CNT,D=30"
1101+48W1*	11 1 18.67 0.27	48 36 47.1 3.6	2.377	42.5 5.1	5				175	118	CNT
1101+48W1A	11 1 18.74 0.32	48 37 23.3 4.2	2.403	14.4 3.6	1						
1101+48W1B	11 1 18.90 0.17	48 36 31.9 2.3	2.375	20.2 4.8	1						
1101+49W1	11 1 13.42 0.30	49 28 45.2 3.9	2.242	27.1 4.8	2				15	117	D=30"
1101+49W2	11 1 19.79 0.11	49 12 21.5 1.4	2.111	19.1 2.6	1					119	
1101+49W3	11 1 33.76 0.02	49 44 35.6 0.3	7.369	262.2 8.0	3	0.975	0.58			123	
1101+49W4	11 1 46.51 0.11	49 4 11.1 1.4	4.448	37.6 5.6	1					125	
1101+50W1	11 1 21.20 0.02	50 56 59.4 0.3	1.388	100.1 4.7	4	0.880	0.50	11		120	HALO?
1101+51W1	11 1 7.67 0.08	51 2 36.5 1.0	1.567	29.4 3.8	4	0.781	0.70	15	130	113	
1101+51W2	11 1 43.36 0.02	51 4 2.6 0.3	2.238	93.9 7.9	3	1.062	0.53			124	
1101+52W1	11 1 13.18 0.28	52 51 0.6 3.2	1.245	9.1 2.2	1						
1101+52W2	11 1 13.86 0.21	52 49 28.6 2.4	1.176	19.4 3.4	4	0.677	0.70	19	40		
1102+47W1	11 2 15.89 0.03	47 9 31.9 0.4	1.501	66.7 1.8	3	0.987	0.36				
1102+47W2*	11 2 20.36 0.10	47 35 15.2 1.3	1.278	66.5 2.7	5				90	129	CNT
1102+47W2A	11 2 18.40 0.26	47 35 13.8 3.5	1.274	11.5 1.9	1						
1102+47W2B	11 2 20.39 0.09	47 35 14.3 1.2	1.277	46.0 3.2	1						
1102+47W2C	11 2 22.31 0.44	47 35 15.0 5.9	1.282	10.2 2.6	1						
1102+47W3	11 2 32.38 0.02	47 24 47.9 0.3	1.029	81.4 1.4	3	0.951	0.42				
1102+50W1	11 2 51.32 0.10	50 39 56.6 1.2	2.436	38.3 6.0	4	0.724	0.70	19	20	137	
1102+52W1	11 2 59.90 0.08	52 38 11.8 0.9	2.019	24.9 2.2	3	1.149	0.58				
1103+47W1	11 3 7.79 0.03	47 49 22.9 0.4	3.625	83.5 3.9	3	0.952	0.58			141	
1103+47W2	11 3 32.60 0.02	47 4 33.2 0.3	3.251	306.8 8.3	4	0.963	0.66	5		144	
1103+47W3	11 3 50.53 0.03	47 38 18.8 0.4	2.734	117.9 2.9	3	0.988	0.58			150	
1103+48W1	11 3 23.68 0.26	48 7 51.9 3.5	1.423	11.6 2.5	1					143	
1103+49W1	11 3 30.97 0.04	49 40 47.0 0.4	1.370	20.5 1.5	3	0.878	0.58				
1103+50W1	11 3 7.91 0.02	50 4 26.9 0.3	3.421	163.8 8.2	4	0.926	0.70	7		140	
1103+50W2	11 3 45.10 0.07	50 28 53.5 0.8	2.006	19.1 2.5	1					148	
1103+52W1	11 3 18.09 0.13	52 54 37.5 1.5	3.843	86.3 9.5	4	0.726	0.93	18	145		
1103+53W1	11 3 22.16 0.06	53 1 9.8 0.6	6.675	221.1 9.2	3	0.959	0.78				
1104+47W1	11 4 3.73 0.06	47 58 18.3 0.8	1.333	22.0 3.2	4	0.817	0.58	12	60	154	
1104+49W1	11 4 33.97 0.09	49 49 40.9 1.2	1.037	20.4 2.6	4	0.657	0.81	20	135	160	
1104+50W1	11 4 2.36 0.07	50 2 8.1 0.9	1.892	22.7 2.0	3	1.108	0.58			153	
1104+50W2	11 4 2.85 0.10	50 38 14.2 1.2	1.237	13.9 3.1	4	0.700	0.58	19			
1104+50W3	11 4 11.66 0.08	50 48 20.7 1.0	1.192	14.7 1.5	1					157	
1104+50W4	11 4 12.19 0.07	50 26 49.5 0.8	1.903	25.0 2.1	3	1.008	0.58			156	
1104+50W5	11 4 19.90 0.15	50 45 26.4 1.8	1.100	12.8 2.8	4	0.586	0.58	25	170	159A	
1104+50W6	11 4 42.40 0.02	50 40 12.0 0.3	1.033	99.7 1.5	3	0.986	0.96			161	
1104+50W7	11 4 52.42 0.08	50 57 21.1 1.0	1.494	16.5 1.9	1						
1104+51W1	11 4 2.75 0.09	51 38 29.4 1.0	2.363	27.4 3.0	1						
1104+51W2	11 4 5.31 0.22	51 54 53.2 2.6	7.732	50.6 9.7	1						
1104+51W3	11 4 21.95 0.07	51 30 59.5 0.8	1.624	22.1 1.7	3	0.944	0.58				

Table 4 (continued)

NAME	RA(1950.0)	DEC(1950.0)	ATTEN	S1415(MFU)	SCODE	Q	QE	PSI	PHI	5C2.	REMARKS
1104+51W4	11 4 52.28 ± 0.19	51 38 57.7 ± 2.3	1.499	10.0 ± 1.9	1						
1104+52W1	11 4 32.01 0.06	52 35 46.4 0.7	9.940	134.0 10.7	3	0.936	0.58				
1105+48W1	11 5 14.47 0.05	48 27 41.5 0.6	2.183	64.9 5.4	4	0.734	0.70	15	110	162	
1105+48W2	11 5 42.85 0.07	48 48 21.5 1.0	2.241	26.7 2.8	1					165	
1105+49W1	11 5 25.03 0.10	49 43 32.2 1.3	1.086	16.8 2.7	4	0.791	0.70	13	115	163	
1105+49W2	11 5 43.59 0.15	49 32 20.4 1.9	1.669	11.7 2.5	1					166	
1105+50W1	11 5 27.22 0.20	50 41 51.2 2.4	1.029	6.8 1.3	1						
1105+50W2	11 5 33.23 0.10	50 36 47.9 1.2	1.119	10.8 1.2	3	0.783	0.58			164	
1105+51W1	11 5 4.96 0.15	51 31 6.8 1.8	1.169	15.5 1.4	3	0.854	0.70				
1105+51W2	11 5 20.15 0.53	51 34 6.0 6.3	1.128	8.2 2.3	1						
1105+51W3	11 5 33.92 0.25	51 34 38.7 2.9	1.089	7.0 1.6	1						
1105+51W4	11 5 40.40 0.17	51 10 57.0 2.1	2.026	14.1 2.5	1						
1105+51W5	11 5 59.64 0.24	51 18 38.8 3.0	1.248	11.6 2.2	1						
1106+48W1	11 6 34.84 0.06	48 39 36.3 0.7	1.536	21.2 1.7	3	0.834	0.50			173	
1106+48W2	11 6 45.02 0.17	48 40 44.0 2.3	1.372	10.2 1.7	1						
1106+48W3	11 6 50.21 0.03	48 58 54.8 0.4	1.409	33.2 1.9	3	0.928	0.50			175	
1106+48W4	11 6 54.28 0.18	48 54 20.1 2.3	1.200	8.2 1.8	1					177	
1106+48W5	11 6 54.55 0.13	48 43 35.1 1.7	1.201	44.0 4.9	4	0.657	0.72	19	120	176	
1106+48W6*	11 6 56.84 0.18	48 51 34.2 2.3	1.136	89.2 4.5	5				10	178	
1106+48W6A	11 6 56.11 0.10	48 50 47.2 1.3	1.133	12.5 1.4	1						
1106+48W6B	11 6 56.94 0.05	48 51 40.4 0.6	1.137	76.7 4.0	1						
1106+50W1	11 6 59.84 0.09	50 46 28.5 1.1	2.013	20.5 2.5	1					179	
1106+51W1	11 6 1.00 0.18	51 7 52.0 2.2	2.562	25.6 3.1	3	0.851	0.70				
1106+51W2	11 6 13.22 0.04	51 46 51.0 0.4	1.814	30.5 2.0	3	1.000	0.58				
1106+51W3	11 6 16.55 0.09	51 40 24.2 1.0	1.261	13.6 1.6	1						
1106+51W4	11 6 22.72 0.04	51 37 13.1 0.4	1.135	50.0 1.7	3	1.001	0.93			172	
1106+51W5	11 6 41.88 0.06	51 21 4.4 0.6	1.223	34.6 3.5	4	0.752	0.70	17	40	174	
1106+51W6	11 6 50.60 0.02	51 45 31.9 0.3	1.844	113.0 2.3	3	1.034	0.70				
1106+51W7	11 6 52.27 0.25	51 25 28.1 3.0	1.149	26.4 3.5	1						
1107+48W1	11 7 9.02 0.14	48 43 55.2 1.8	1.118	10.1 1.4	3	0.732	0.70				
1107+48W2	11 7 45.98 0.02	48 34 10.4 0.3	1.529	551.1 4.7	3	1.010	0.87			183	
1107+48W3	11 7 47.00 0.17	48 20 34.2 2.3	5.343	61.5 7.3	3	0.906	0.81			184	
1107+48W4*	11 7 53.74 0.48	48 3 23.8 6.6	8.487	96.3 18.2	5				90	185	D=45"
1107+48W4A	11 7 51.23 0.30	48 3 22.0 4.1	8.016	46.1 12.0	1						
1107+48W4B	11 7 55.65 0.36	48 3 24.4 4.9	8.872	44.4 13.3	1						
1107+49W1	11 7 57.56 0.15	49 0 25.9 1.9	1.290	16.8 2.3	1					186	
1107+51W1	11 7 21.18 0.17	51 40 14.4 2.1	1.668	19.0 2.1	3	0.894	0.70				
1108+48W1	11 8 8.53 0.27	48 47 44.7 3.5	1.030	6.5 1.5	1						
1108+48W2	11 8 31.58 0.05	48 37 4.5 0.6	1.472	27.4 1.6	3	0.961	0.58				
1108+49W1*	11 8 4.20 0.14	49 11 13.3 1.9	2.763	145.0 12.4	5				10	187	CNT
1108+49W1A	11 8 4.03 0.17	49 10 48.5 2.3	2.657	42.5 6.6	1						
1108+49W1B	11 8 4.34 0.25	49 11 20.7 3.2	2.796	102.1 9.8	1						
1108+50W1	11 8 23.77 0.18	50 25 41.8 2.2	1.131	8.9 1.7	1						
1108+51W1	11 8 37.73 0.13	51 18 0.4 1.6	1.228	9.1 1.5	1						
1109+48W1*	11 9 29.32 0.34	48 12 26.1 4.5	5.305	228.1 31.8	5				75	194	CNT
1109+48W1A	11 9 25.68 0.42	48 12 16.8 5.7	5.707	94.2 22.8	1						

Table 4 (continued)

NAME	RA(1950.0)	DEC(1950.0)	ATTEN	S1415(MFU)	SCODE	Q	QE	PSI	PHI	5C2.	REMARKS
1109+48W1B	11 9 31.06 ± 0.34	48 12 30.0 ± 4.6	5.130	115.4±20.5	1						
1109+48W2	11 9 35.63 0.23	48 31 45.7 3.0	2.674	17.0 3.3	1						
1109+49W1	11 9 8.75 0.09	49 13 19.8 1.1	3.093	34.2 3.9	1					189	
1109+49W2	11 9 9.79 0.13	49 53 1.3 1.5	1.768	17.6 2.2	3	0.851	0.70			190	
1109+49W3	11 9 12.60 0.08	49 40 39.1 0.9	1.058	15.0 1.3	3	1.051	0.70				
1109+49W4*	11 9 12.97 0.36	49 55 57.2 4.5	2.183	56.7 5.5	5				55	191	CNT
1109+49W4A	11 9 11.16 0.10	49 55 50.6 1.2	2.174	39.1 3.3	1						
1109+49W4B	11 9 16.37 0.24	49 56 22.6 2.9	2.243	17.4 2.8	1						
1109+49W5	11 9 24.44 0.15	49 25 36.0 1.9	1.258	11.6 1.6	1					193	
1109+49W6	11 9 32.95 0.15	49 2 51.2 1.9	2.778	20.7 3.5	1					195	
1109+49W7	11 9 33.05 0.15	49 38 17.4 1.9	1.006	8.2 1.3	1						
1109+50W1	11 9 4.25 0.21	50 13 33.3 2.7	1.384	38.1 6.9	2				125	188	CNT,D=40"
1109+50W2	11 9 16.39 0.11	50 4 13.5 1.3	2.720	26.0 3.4	1					192	
1109+50W3	11 9 40.61 0.03	50 29 36.2 0.4	1.048	76.4 2.5	4	0.893	0.58	9	95	196	
1109+51W1	11 9 9.01 0.15	51 16 33.1 1.8	1.088	9.2 1.4	1						
1109+51W2	11 9 10.52 0.14	51 39 33.7 1.6	2.077	23.3 2.6	1						
1109+51W3	11 9 20.00 0.11	51 16 49.2 1.3	1.054	14.9 1.4	3	1.014	0.81				
1109+51W4	11 9 50.68 0.35	51 22 7.7 4.2	1.005	7.1 1.8	1						
1110+49W1	11 10 9.32 0.29	49 58 47.1 3.2	2.896	30.0 5.1	1						
1110+49W2	11 10 38.46 0.13	49 33 8.9 1.6	1.237	12.9 1.9	1						
1110+49W3	11 10 45.91 0.07	49 56 56.5 0.8	3.020	38.0 3.3	3	0.864	0.58				
1110+49W4	11 10 54.02 0.05	49 33 55.5 0.6	1.373	35.6 1.7	3	0.964	0.70			201	
1110+49W5	11 10 55.64 0.11	49 25 7.2 1.5	1.788	18.6 2.2	3	0.804	0.70			202	
1110+50W1	11 10 17.24 0.07	50 10 4.8 0.9	2.077	26.0 2.3	3	0.887	0.56				
1110+50W2	11 10 50.62 0.45	50 33 21.3 5.8	1.722	27.7 5.2	2					200	
1110+51W1	11 10 15.83 0.05	51 45 53.6 0.5	3.762	377.8 10.0	4	0.836	1.51	13	0	198	
1110+51W2	11 10 22.25 0.18	51 17 8.9 2.3	1.104	8.1 1.4	1						
1111+48W1	11 11 2.33 0.10	48 33 9.4 1.3	1.147	14.1 1.4	3	1.068	0.70				
1111+48W2	11 11 21.66 0.10	48 35 28.8 1.3	1.118	47.9 6.9	4	0.423	0.80	26	70	203	CNT
1111+48W3	11 11 28.58 0.09	48 45 17.9 1.2	1.714	37.2 4.2	4	0.823	0.93	13	80	207	
1111+48W4	11 11 49.61 0.36	48 16 30.2 4.7	1.345	17.6 2.9	2						
1111+48W5	11 11 56.44 0.10	48 44 39.2 1.4	1.615	24.3 1.7	3	1.048	0.58				
1111+49W1	11 11 10.01 0.08	49 47 40.5 0.9	2.023	25.6 2.2	3	0.925	0.58				
1111+50W1	11 11 22.10 0.15	50 55 53.2 1.8	6.210	72.7 9.3	1					204	
1111+50W2	11 11 24.19 0.06	50 37 30.3 0.7	3.002	38.7 4.5	1					205	
1111+51W1*	11 11 25.91 0.44	51 9 10.8 5.3	2.238	156.6 15.6	5				10	206	CNT
1111+51W1A	11 11 25.63 0.17	51 8 44.8 2.1	2.281	76.4 9.1	1						
1111+51W1B	11 11 26.23 0.36	51 9 38.2 4.4	2.196	80.1 13.2	1						
1112+48W1	11 12 5.63 0.11	48 33 59.0 1.4	1.062	13.8 1.3	3	1.064	0.70				
1112+48W2	11 12 40.10 0.24	48 38 33.7 3.1	1.371	9.3 1.7	1						
1112+48W3	11 12 42.32 0.29	48 25 19.7 3.9	1.192	8.0 1.5	1						
1112+48W4	11 12 42.72 0.03	48 20 13.4 0.4	1.354	31.3 1.7	3	1.092	0.70				
1112+48W5	11 12 52.39 0.26	48 50 41.5 3.4	3.279	36.0 5.1	3	0.765	1.05				
1112+50W1	11 12 23.52 0.05	50 25 24.1 0.5	6.565	179.4 7.1	3	1.073	0.58				
1113+48W1	11 13 22.84 0.07	48 47 27.5 0.9	3.298	40.7 3.6	3	1.021	0.56				
1113+48W2	11 13 23.25 0.77	48 33 2.6 9.9	1.676	19.7 3.6	2						

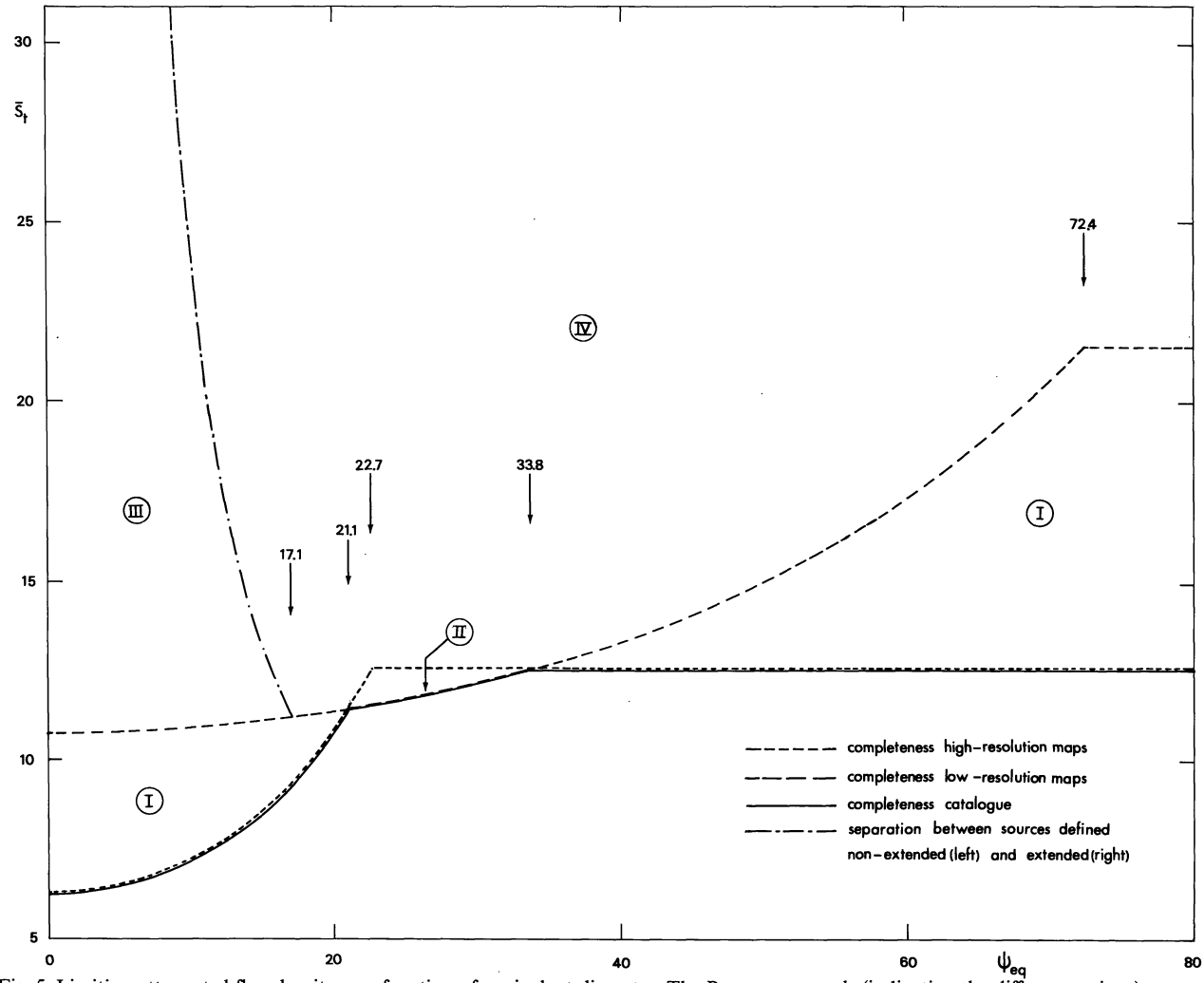

Fig. 5. Limiting attenuated flux density as a function of equivalent diameter. The Roman numerals (indicating the different regions) correspond to the flux density code given in the source list. For a detailed explanation we refer to the text (Section VI)

VI. Completeness of the Source List

Because the present source list will be used for statistical work, it is essential to determine its completeness. By completeness we mean that all sources satisfying certain criteria are included in the source list (and none other). The criteria that are relevant for the completeness of a ("monochromatic") source list concern flux density and equivalent diameter. More specifically: one must determine the limiting flux density above which all sources with a given equivalent diameter have been included in the source list.

Ideally, this limiting flux density should be a noise-free, real-sky flux density while the equivalent diameter should be a noise-free, unbiased measure of the real angular size. In practice however, we can only discuss completeness in terms of attenuated flux density estimates and estimated equivalent diameter (based on an equal double source model).

The discussion of completeness is relatively simple when we express completeness in terms of estimated parameters. We then need only transform the limiting values of $\bar{S}_h$ and $\bar{S}_l$ into a limiting value of $\bar{S}_t$ as a function of Ψ_{eq}. The procedure is illustrated in Fig. 5, where we have plotted $\bar{S}_t$ as a function of Ψ_{eq}. The two dashed curves indicate $\bar{S}_{h,\lim} \exp(0.00135\ \Psi_{eq}^2)$ and $\bar{S}_{l,\lim} \exp(0.000132\ \Psi_{eq}^2)$ for $\bar{S}_{h,\lim} = 6.25$ m.f.u. and $\bar{S}_{l,\lim} = 10.75$ m.f.u. Beyond $\Psi_{eq} = 22''.7$ and $72''.4$ respectively, i.e. where an equal double source will become resolved by the two beams, $\bar{S}_t$ was taken to be constant and equal to $2\,\bar{S}_{h,\lim}$ and $2\,\bar{S}_{l,\lim}$ respectively. This ratio $\bar{S}_t/\bar{S}_{\lim}$ for separations larger than the respective beamwidths depends clearly on the source model. For unequal double sources this ratio will generally be less than two. Also, the location of the dashed curves will be slightly different for unequal double sources.

On the assumption of the equal double source model, however, the completeness of the source list is given by the solid line. Quantitatively, the completeness can therefore be described as follows:

$$\Psi_{eq} \leqq 21''.1 : \bar{S}_{t,\lim} = 6.25 \exp(0.00135\ \Psi_{eq}^2) \text{ m.f.u.}$$

$$21''.1 < \Psi_{eq} \leqq 33''.8 : \bar{S}_{t,\lim} = 10.75 \exp(0.000132\ \Psi_{eq}^2) \text{ m.f.u.}$$

$$33''.8 < \Psi_{eq} : \bar{S}_{t,\lim} = 12.50 \text{ m.f.u.}$$

It must be stressed that the completeness of the source list, as given above, refers only to the inclusion of sources with a given total flux density and diameter. Consequently, these completeness limits can not be applied to the flux densities in the source list, because the flux density estimates ($\bar{S}$) given in the source list are not necessarily identical to $\bar{S}_t$. As a matter of fact, only for sources in Region IV (see Fig. 5) do $\bar{S}$ and $\bar{S}_t$ coincide. For sources in the Regions I, II and III $\bar{S}$ is smaller than $\bar{S}_t$. The ratio between $\bar{S}$ and $\bar{S}_t$ (which is a function of Ψ_{eq}) depends on the flux density code (1, 2 or 3), i.e. on the region in the $(\bar{S}_t, \Psi_{eq})$-plane (I, II or III). A statistical correction from $\bar{S}$ to $\bar{S}_t$ can only be applied when the angular diameter distribution is known.

VII. Detection of 5C2 Sources

Information on the detection of 5C2 sources has implicitly been given in Column 11 of Table 4. For easy reference, we have also made a list of all 5C2 sources within the 10 dB attenuation contours of the twenty-four fields. This list (cf. Table 5) contains 190 5C2 sources,

Table 5. Detection of 5C2 sources

1[c])	22[c])	42[a])	62[a])	81[b])	103[c])	129[a,d])	157[a])	178[a])	198[a,d])
2[a,d])	23[b])	43[a])	63[c])	82[a,d])	104[a])	131[c])	159a[a])	179[a])	199[b])
3[c,d])	24[b])	44[a,d])	64[a])	83[c])	105[c])	132[c])	159b[b])	180[b])	200[a,d])
4[a,d])	25[a])	45[a])	65[a])	84[b])	107[c])	134[c])	160[a])	181[b])	201[a])
5[a,d])	26[a])	46[a])	66[a])	85[a])	109[a])	135[c])	161[a])	182[c])	202[a])
7[a])	27[b])	47[a])	67[a])	86[a])	110[a])	136[c])	162[a])	183[a])	203[a,d])
8[a])	28[c])	48[a])	68[c])	87[a])	111[c])	137[a])	163[a])	184[a])	204[a,d])
9[a])	29[a])	49[b])	69[c])	88[a])	112[c])	140[a])	164[a])	185[a,d])	205[a,d])
10[a])	30[a])	50[a,d])	70[b])	89[b])	113[a])	141[a,d])	165[a])	186[a])	206[a,d])
11[a])	31[c])	51[c])	71a[c])	91[a])	114[b])	142[c])	166[a])	187[a])	207[a,d])
12[a,d])	32[c])	52[b])	71b[c])	92[a,d])	116[c])	143[a])	167[c])	188[a])	
13[a])	33[a])	53[a])	72[a])	93[c])	117[a])	144[a,d])	168[c])	189[a])	
14[a])	34[a])	54[a])	73[a])	94[a])	118[a])	146[c])	169[c])	190[a])	
15[a,d])	35[b])	55[a])	74[a])	95[c,d])	119[a])	148[a])	171[b])	191[a])	
16[a])	36[a])	56[a])	75[a])	96[b])	120[a])	150[a,d])	172[a,d])	192[a])	
17[a,d])	37[b,d])	57[a,d])	76[c])	97[a,d])	123[a])	152[c])	173[a])	193[a])	
18[a])	38[a])	58[a])	77[a])	98[b])	124[a])	153[a])	174[a,d])	194[a,d])	
19[a])	39[a])	59[a])	78[a])	99[a])	125[a])	154[a])	175[a])	195[a])	
20[b])	40[a])	60[c])	79[a])	100[c])	126[a,d])	155[c])	176[a])	196[a])	
21[a])	41[c])	61[a])	80[b])	101[b])	127[c])	156[a])	177[a])	197[c])	

[a]) Detected, source belongs to complete sample at 1415 MHz.
[b]) Detected, source does not belong to complete sample at 1415 MHz.
[c]) Not detected.
[d]) Source does not belong to complete sample at 408 MHz.

Table 6. Possible detections of additional 5C2-sources

5C2.	RA(1950.0)	DEC(1950.0)	ATTEN	S1415(MFU)	SCODE
20	10 51 33.37 ± 0.18	50 17 56.1 ± 2.3	2.428	11.3 ± 3.0	1
23	10 52 5.80 0.53	49 45 42.0 6.6	2.357	21.1 5.1	2
24	10 52 6.22 0.26	49 22 3.5 3.4	1.659	10.0 2.1	1
27	10 52 46.36 0.46	49 20 44.0 5.7	1.735	16.2 3.7	2
35	10 53 52.23 0.40	50 13 55.4 4.9	2.041	11.4 2.6	1
37	10 53 58.66 0.28	47 53 27.6 3.7	5.942	33.3 7.5	1
49	10 54 42.42 0.47	50 25 15.1 5.5	1.084	9.7 2.3	2
52	10 55 9.23 0.26	50 11 52.6 3.2	1.483	7.9 1.8	1
70	10 56 25.83 0.64	51 0 39.5 7.7	1.949	19.0 4.2	2
80	10 57 45.17 0.27	51 8 30.3 3.2	1.788	10.5 2.2	1
81	10 57 52.39 0.15	48 43 16.6 1.8	1.771	8.3 2.2	1
84	10 58 22.99 0.13	50 53 8.3 1.4	1.752	9.9 2.2	1
89	10 58 35.69 0.26	50 54 57.1 3.3	1.581	9.6 2.0	1
96	10 59 14.35 0.25	48 49 29.1 3.2	1.699	8.8 2.1	1
98	10 59 34.04 0.54	50 30 50.4 6.7	2.300	20.1 4.9	2
101	10 59 45.39 0.49	48 41 52.6 6.4	1.214	7.1 2.6	2
114	11 1 8.66 0.15	49 3 3.0 2.1	2.829	17.0 3.5	1
159B	11 4 31.35 0.19	50 47 14.0 2.4	1.081	6.0 1.3	1
171	11 6 7.67 0.39	48 49 3.5 5.1	1.648	10.0 2.5	1
180	11 7 2.88 0.13	50 20 5.2 1.6	2.653	16.3 3.3	1
181	11 7 15.95 0.23	49 22 31.4 2.9	4.334	24.3 5.4	1
199	11 10 26.51 0.53	50 8 30.5 6.4	2.488	25.6 5.3	2

40 (i.e. 21 %) of which could not be detected at 1415 MHz. From the remaining 150 sources, 128 are included in the source list (i.e. they have $\bar{S}_h \geqq 6.25$ m.f.u. and/or $\bar{S}_l \geqq 10.75$ m.f.u.). Information on the remaining 22 sources (which have $\bar{S}_h \leqq 6.25$ m.f.u. and/or $\bar{S}_l \leqq 10.75$ m.f.u.) is given in Table 6, which has essentially the same organization as Table 4. We consequently refer to Section V (Column 11 and Columns 2–6) for the explanation of the data in Table 6.

Those 5C2 sources which, at 408 MHz, have an attenuation factor larger than 5.0 have been indicated by d) in Table 5. Excluding such sources, the list contains 159 sources, of which 38 have not been detected. Twentyone sources with a 408 MHz attenuation less than 5.0 were detected, but are not in the source list. The remaining 100 sources constitute a sample with well-defined completeness limits at both frequencies from which unbiased spectral index information may be derived.

VIII. Comparison with Other Observations of the 5C2 Region

The 5C2 region has been observed at several other frequencies. Apart from the present 1415 MHz observations there are:

a) observations with the Cambridge One-Mile telescope at frequencies of 408 and 1407 MHz, with a limiting attenuated flux density of about 12 m.f.u. at both frequencies (Pooley and Kenderdine, 1968)

b) observations with the N.R.A.O. 300-ft telescope at a frequency of 1400 MHz, with a limiting flux density of about 90 m.f.u. (Maslowski, 1972)

c) observations with the N.R.A.O. 140-ft telescope at a frequency of 5000 MHz, with a limiting flux density of about 90 m.f.u. (Pauliny-Toth *et al.*, 1972)

d) photographic observations in U, B and V with the 134/200 cm Schmidt telescope of the Karl Schwarzschild Observatory at Tautenburg, with a limiting magnitude of about 20^m in the three colours (Notni *et al.*, 1971).

A comparison between the 408 MHz radio positions and the optical positions has already been made by Notni *et al.* Here we will only make a comparison between the 408 MHz positions and the 1415 MHz positions from the present survey. In Figs. 6a–6d we have plotted $\Delta\alpha(=\alpha_{408}-\alpha_{1415})$ and $\Delta\delta(=\delta_{408}-\delta_{1415})$, both against r_α and r_δ where r_α and r_δ denote distances from the 408 MHz field centre along great circles. It is immediately clear that the two positional systems are not identical. Obviously, the scales in right ascension direction differ appreciably, but even more striking is the dependence of $\Delta\alpha$ on r_δ and that of $\Delta\delta$ on r_α.

It appears that the behaviour of the four functions displayed in Figs. 6a–6d can be explained most simply by incorrect precession corrections in the Cambridge 408 MHz measurements (i.e. apart from possible differences in zero point). In this explanation, where it is assumed that no differential precession correction was applied to the 408 MHz positions, one expects (in first order approximation) a linear compression in right ascension direction and a rotation of the coordinate system. The magnitudes of these effects have been indicated by solid lines in Figs. 6a–6d, i.e. these solid lines are *not* least squares solutions fitted to the observational data. It can be seen that these predictions agree very well with the experimental data. However, Dr. Pooley (private communication) is almost certain that differential precession has been allowed for in the Cambridge 408 MHz observations and he thinks that the systematic effects in Figs. 6a–6d must be explained in some other way.

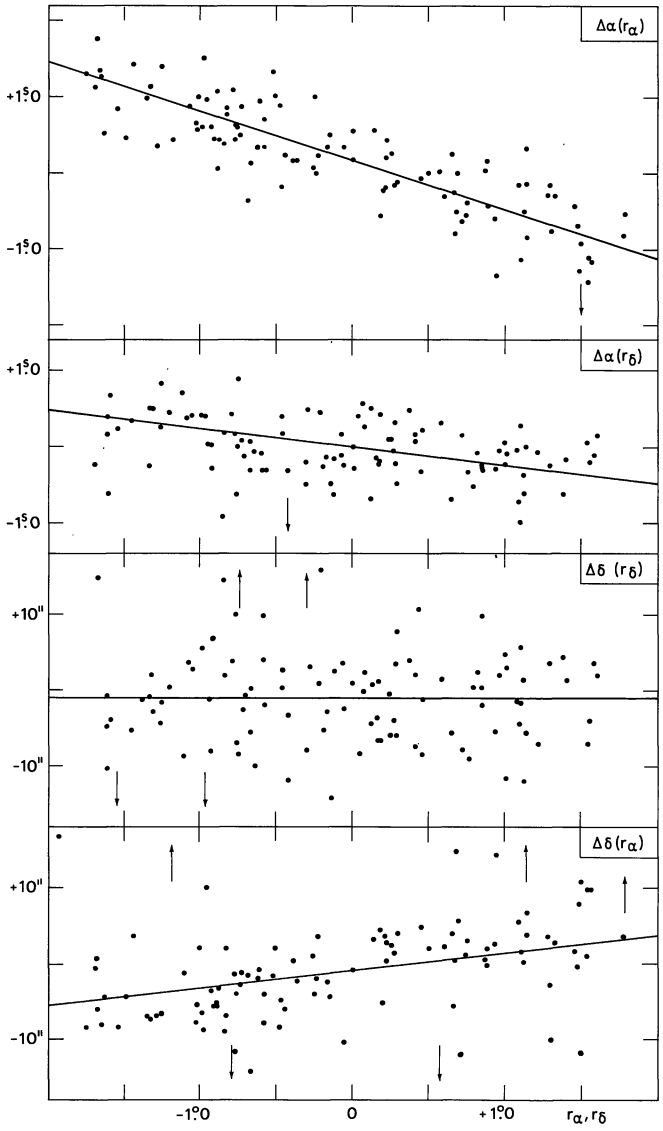

Fig. 6. Position differences (Cambridge 408 MHz minus Westerbork 1415 MHz) for all 5C2 sources belonging to the complete sample defined at 1415 MHz. The values of $\Delta\alpha(r_\delta)$ have been corrected for the general slope in $\Delta\alpha(r_\alpha)$ as given by the solid line in (a). Note that the solid lines do *not* represent least squares fits to the points

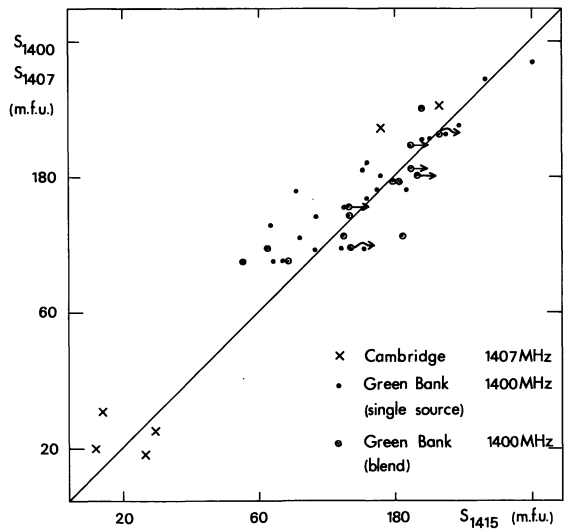

Fig. 7. The Cambridge 1407 MHz and Green Bank 1400 MHz flux densities versus the Westerbork 1415 MHz flux densities. Arrows indicate lower limits to the 1415 MHz flux density for 1400 MHz blends of several sources not all of which were detected at 1415 MHz

The dependence of $\Delta\alpha$ on r_α was also found by Notni *et al.* when analyzing the differences between the optical and radio positions. It seems that these authors interpreted this effect as a frequency (or baseline-length) error in the Cambridge measurements, because they applied an analogous correction to the radio declinations. However, the absence of a dependence of $\Delta\delta$ on r_δ (cf. Fig. 6c) rules out such an explanation. Moreover, such an explanation would imply a frequency error of about 700 kHz or, alternatively, a baseline-length error of about 3 m, both of which are practically impossible.

In Fig. 7 we have plotted Cambridge 1407 MHz and Green Bank 1400 MHz flux densities against 1415 MHz flux densities for sources common to the three catalogues. Because of the limited number of sources common to the Cambridge 1407 MHz and the present 1415 MHz survey very little can be said about the relationship between the two flux density scales. The situation is different for the Green Bank and Westerbork flux density scales. It seems as if the 1400 MHz Green Bank flux densities below about 150 m.f.u. have been systematically overestimated (on the average 20% for flux densities of about 90 m.f.u.) with respect to the Westerbork 1415 MHz flux densities. This must, at least partly, be due to the considerable difference in beam area: the Westerbork low-resolution beam has an area that is about 60 times smaller than that of the Green Bank beam. For the stronger sources the two flux density scales seem to agree satisfactorily.

Acknowledgements. Thanks are due to the staff of the Westerbork Radio Observatory for their assistance in obtaining the qualitatively homogeneous observations and to the reduction group, in particular Messrs. J. W. Brotherhood and H. W. van Someren Gréve, for their indispensable assistance in the handling of more than 400 jobs.
The observations were planned and executed in close collaboration with Mr. R. S. Le Poole, who also suggested improvements to an earlier draft of this paper. Throughout this work my wife gave much professional and social assistance without which this work would not have been finished.
Messrs. P. J. den Hoed (drawings) and H. Kleibrink (photography) assisted in making the manuscript ready for publication.
The Westerbork Radio Observatory is operated by the Netherlands Foundation for Radio Astronomy with the financial support of the Netherlands Organization for the Advancement of Pure Research (Z.W.O.).

References

Brouw, W.N. 1971, Data Processing for the Westerbork Synthesis Radio Telescope, Thesis Leiden University
Katgert, J.K., Spinrad, H. 1974, *Astron. & Astrophys.* **35**, 393
Katgert, P., Katgert-Merkelijn, J.K., Le Poole, R.S., Van der Laan, H. 1973, *Astron. & Astrophys.* **23**, 171
Maslowski, J. 1972, *Astron. & Astrophys.* **16**, 197
Notni, P., Oleak, H., Richter, G.M. 1971, *Astron. Nachr.* **293**, 221
Pauliny-Toth, I.I.K., Kellermann, K.I., Davis, M.M., Fomalont, E.B., Shaffer, D.B. 1972, *Astron. J.* **77**, 265
Pooley, G.G., Kenderdine, S. 1968, *Monthly Notices Royal Astron. Soc.* **139**, 529
Pooley, G.G., Ryle, M. 1968, *Monthly Notices Royal Astron. Soc.* **139**, 515

P. Katgert
Institute of Astronomy
Madingley Road
Cambridge CB3 OHA
England